of C/EBPβ was decreased but not totally blocked in the *Erk1/2*$^{gc-/-}$ mice (fig. S8, B and C), indicating that C/EBPβ expression is regulated by additional pathways and that ERK1/2-mediated phosphorylation and activation of C/EBPβ is critical. Thus, C/EBPβ is a downstream effector of ERK1/2 in GCs during ovulation and luteinization. The lower penetrance of ovulation and gene expression defects in *Cebpb*$^{gc-/-}$ mice, compared with the *Erk1/2*$^{gc-/-}$ mice, suggests that C/EBPβ is one, but not the only, critical transcription factor regulated by ERK1/2 in vivo.

The *Erk1/2*$^{gc-/-}$ mouse model illustrates that disruption of *Erk1/2* in GCs in vivo completely derails the ability of LH to induce genes controlling ovulation, COC expansion, oocyte maturation, and luteinization without altering genes that regulate normal follicular development to the preovulatory stage (summarized in Fig. 4D). As a consequence of ERK1/2 depletion in GCs, the FSH program is extended rather than being abruptly terminated by LH/hCG. Thus, our results demonstrate in animals that the critical roles of ERK1/2 in GCs are highly selective and cell context–specific, confirming findings of in vitro studies (*6*, *18*). Moreover, ERK1/2 are activated for a relatively short period of time (from 0.5 to 2 hours) in GCs of the preovulatory follicles exposed to LH/hCG (*11*, *12*, *19*), and this brief window of activation is necessary and sufficient to reprogram preovulatory GCs to cease dividing and terminally differentiate.

The effect of ERK1/2 activation in GCs of preovulatory follicles but not in follicles at earlier stages of growth indicates that activation of these kinases is controlled tightly by specific mechanisms. Indeed, inappropriate activation of ERK1/2 in GCs of small growing follicles might disrupt normal follicular development because mice in which ovarian GCs express a constitutively active K-RAS mutant suffer impaired follicle development and premature ovarian failure (*11*). Thus, further understanding of the molecular mechanisms by which ERK1/2 regulate ovarian cell functions will help unravel some of the causes of ovarian pathologies and cancer, as well as lead to therapies for female infertility.

References and Notes

1. M. Hunzicker-Dunn, E. T. Maizels, *Cell. Signal.* **18**, 1351 (2006).
2. M. M. Matzuk, K. H. Burns, M. M. Viveiros, J. J. Eppig, *Science* **296**, 2178 (2002).
3. J. Y. Park *et al.*, *Science* **303**, 682 (2004).
4. M. Hsieh *et al.*, *Mol. Cell. Biol.* **27**, 1914 (2007).
5. M. Shimada, I. Hernandez-Gonzalez, I. Gonzalez-Robayna, J. S. Richards, *Mol. Endocrinol.* **20**, 1352 (2006).
6. Y. Q. Su, K. Wigglesworth, F. L. Pendola, M. J. O'Brien, J. J. Eppig, *Endocrinology* **143**, 2221 (2002).
7. Z. Chen *et al.*, *Chem. Rev.* **101**, 2449 (2001).
8. G. Pages *et al.*, *Science* **286**, 1374 (1999).
9. M. Aouadi, B. Binetruy, L. Caron, Y. Le Marchand-Brustel, F. Bost, *Biochimie* **88**, 1091 (2006).
10. A. M. Fischer, C. D. Katayama, G. Pages, J. Pouyssegur, S. M. Hedrick, *Immunity* **23**, 431 (2005).
11. H. Y. Fan *et al.*, *Development* **135**, 2127 (2008).
12. S. Panigone, M. Hsieh, M. Fu, L. Persani, M. Conti, *Mol. Endocrinol.* **22**, 924 (2008).
13. E. Gershon, A. Hourvitz, S. Reikhav, E. Maman, N. Dekel, *FASEB J.* **21**, 1893 (2007).
14. J. S. Richards, *Endocrinology* **142**, 2184 (2001).
15. E. Sterneck, L. Tessarollo, P. F. Johnson, *Genes Dev.* **11**, 2153 (1997).
16. M. Bück, V. Poli, P. vander Geer, M. Chojkier, T. Hunter, *Mol. Cell* **4**, 1087 (1999).
17. E. Sterneck, S. Zhu, A. Ramirez, J. L. Jorcano, R. C. Smart, *Oncogene* **25**, 1272 (2006).
18. S. Sela-Abramovich, E. Chorev, D. Galiani, N. Dekel, *Endocrinology* **146**, 1236 (2005).
19. E. T. Maizels, J. Cottom, J. C. Jones, M. Hunzicker-Dunn, *Endocrinology* **139**, 3353 (1998).

20. We thank J. Pouyssegur and J. Shao for providing *Erk1*$^{-/-}$ mice and adenoviral vector of C/EBPβ, respectively. This work was supported by NIH grants NIH-HD16229, NIH-HD07495, Project II (J.S.R.), Grant-in-Aid for Scientific Research No. 18688016 from the Japan Society for the Promotion of Science (M.S.), Intramural Research Program of NIH, National Cancer Institute, Center for Cancer Research (P.F.J. and E.S.), and NIH Postdoctoral Training Grant NIH-HD07165 (H.-Y.F.). The Gene Expression Omnibus accession number for microarray data is GSE15135.

Supporting Online Material

www.sciencemag.org/cgi/content/full/324/5929/938/DC1
Materials and Methods
Figs. S1 to S8
Tables S1 and S2
References

26 January 2009; accepted 20 March 2009
10.1126/science.1171396

Cell Movements at Hensen's Node Establish Left/Right Asymmetric Gene Expression in the Chick

Jerome Gros,[1] Kerstin Feistel,[2]* Christoph Viebahn,[3] Martin Blum,[2] Clifford J. Tabin[1]†

In vertebrates, the readily apparent left/right (L/R) anatomical asymmetries of the internal organs can be traced to molecular events initiated at or near the time of gastrulation. However, the earliest steps of this process do not seem to be universally conserved. In particular, how this axis is first defined in chicks has remained problematic. Here we show that asymmetric cell rearrangements take place within chick embryos, creating a leftward movement of cells around the node. It is the relative displacement of cells expressing *sonic hedgehog* (*Shh*) and *fibroblast growth factor 8* (*Fgf8*) that is responsible for establishing their asymmetric expression patterns. The creation of asymmetric expression domains as a passive effect of cell movements represents an alternative strategy for breaking L/R symmetry in gene activity.

In mice and rabbits, monocilia found on cells of the posterior notochordal plate have been shown to play a crucial role in breaking left/right (L/R) symmetry (*1*, *2*). These cilia are able to create a leftward flow of fluid in a pit-like teardrop-shaped space that is not covered by subjacent endoderm (*3*). The flow of fluid across this pit stimulates signal transduction that ultimately leads to the induction of asymmetric gene expression (*1*, *2*).

In contrast, in the chick embryo, the endoderm underlying Hensen's node (a structure at the rostral end of the primitive streak in the gastrulating embryo) exists as a continuous sheet ventral to the notochordal plate mesoderm (*4*), and there is no morphological pit on the ventral surface in which a flow of fluid could be established. Essner *et al.* have observed cilia at Hensen's node in earlier work (*5*), but these short cilia are on endodermal cells and are unrelated to the motile cilia on the mesodermal cells of the ventral node in the mouse and rabbit. The mesodermal cells at Hensen's node in the chick are devoid of cilia. In addition, the Talpid chick mutant lacks primary cilia (*6*) but does not exhibit L/R asymmetry defects. Unlike in the mouse and rabbit, the chick node itself becomes morphologically asymmetric, with a marked tilt toward the left around the time the primitive streak reaches full extension at stage 4 (*7*, *8*) (Fig. 1, A to C). Shortly thereafter, a number of small L/R asymmetric expression domains are observed to the right and left of the node (*9*). However, all of the genes expressed in such a manner are initially expressed in a symmetric fashion: for example, *fibroblast growth factor 8* (*Fgf8*) bilaterally along the primitive streak and *sonic hedgehog* (*Shh*) bilaterally across the top of the node until stage 4 (*10*) (Fig. 1, D to G). Subsequently, concomitant with the development of morphological asymmetries in the node, these gene expression patterns also become gradually asymmetric by stage 5 (Fig. 1, H and I).

To investigate cellular rearrangements that could be responsible for establishing the morphological asymmetry of the node, we performed

[1]Department of Genetics, Harvard Medical School, Boston, MA 02115, USA. [2]Institute of Zoology, Hohenheim University, 70953 Stuttgart, Germany. [3]Department of Anatomy and Embryology, Göttingen University, 37079 Göttingen, Germany.

*Present address: Division of Neuroscience, Oregon National Primate Research Center, Oregon Health and Science University, Beaverton, OR 97006, USA.
†To whom correspondence should be addressed. E-mail: tabin@genetics.med.harvard.edu

a time-lapse analysis of cell movements at Hensen's node, randomly labeling cells by electroporation of a green fluorescent protein (GFP) reporter (*11*). At stage 4, as primitive streak elongation terminates (Fig. 1, K and O) but regression has not yet begun (Fig. 1, M and Q), the cells that have formed the node exhibit a definitive, albeit brief (3 to 4 hours), leftward movement [n = 10/10, where n represents the number of embryos analyzed; movies S1 to S3; and Fig. 1, L and P).

We next attempted to block the leftward movement of cells at the node by the use of drugs that inhibit the function of rho kinase (Rok) (Y-27632) and its target myosinII (blebbistatin). These two proteins have been shown to provide the force driving various oriented cell rearrangements in several species. After adding these drugs, gastrulation movements continued (Fig. 1R and fig. S1, B, F, and J), and most reached at least stage 6 when the notochord has formed, although as previously described (*12*, *13*), primitive-streak regression was affected (Fig. 1T and fig. S1, D, H, and L). In these drug-treated embryos, the leftward movements of cells at the node were no longer observed (movies S4 and S5; Fig. 1S; and fig. S1, C, G, and K). Three-dimensional (3D) reconstruction of Hensen's node from stage 5 embryos that were cultured in blebbistatin or Y-27632 revealed that the node displays a more symmetrical and anteriorly extended shape as compared with control embryos (dotted lines; Fig. 2, A, B, E, and F; and fig. S2, A and B), suggesting that the cell movements we identified are responsible for the morphological asymmetry of the node. Moreover, we noted that these embryos also displayed symmetrical expression of *Shh* and FGF8 (Y-27632, n = 16/23; blebbistatin, n = 17/21; Fig. 2, G and H; and fig. S2, C and D).

Additionally, we attempted to block the leftward cell movements anterior to the node by two physical methods: (i) manually inserting individual human hairs through the primitive streak extending anterior to the node and (ii) surgically bisecting the embryos along the midline. Both manipulations also led to bilateral gene expression (fig. S3). Thus, the leftward cellular movements at the node are necessary to initiate L/R asymmetric expression domains in the chick.

It has been previously demonstrated that asymmetric expression of *Shh* and FGF8 depends on a transient, H+/K+ adenosine triphosphatase (ATPase)–dependent depolarization of membrane potential on the left side of the primitive streak, just before stage 4 (*14*). We cultured embryos in plates containing the H+/K+ ATPase inhibitors SCH28080 or omeprazole and found that the node displayed a symmetrical morphology comparable to the phenotypes observed with myosinII and Rok inhibitors, suggesting that in these conditions the cell rearrangements at the node did not occur properly (Fig. 2, I and J, and fig. S2, E and F). Moreover, when we performed a time-lapse analysis on GFP electroporated embryos cultured on plates containing omeprazole, we did not observe any leftward movements at the node (n = 3/4) (movie S6, Fig. 1V, and fig. S1O) as were observed in control embryos (n = 10/10, Fig. 1, L and P, and movie S1), although the primitive streak elongated and regressed normally (Fig. 1, U to W, and fig. S1, N to P). Embryos treated with H+/K+ ATPase inhibitors exhibited symmetrical expression of *Shh* and FGF8 [as previously reported in (*14*)] by stage 5 to 6 (SCH28080, n = 7/12; omeprazole, n = 6/7; Fig. 2, K and L; and fig. S2, G and H). These data show that the leftward movement at the node is downstream of the asymmetric H+/K+ ATPase activity.

The mechanism for setting up L/R asymmetric gene expression patterns at the chick node may have relevance beyond avian species. Despite the morphological conservation of the notochordal plate's ventral surface as seen in mice, rabbits, and possibly humans (*15*), histological analysis reveals that, similar to the chick, the cells of the pig notochordal plate do not contain cilia (Fig. 3, A to C, and fig. S4, D to J).

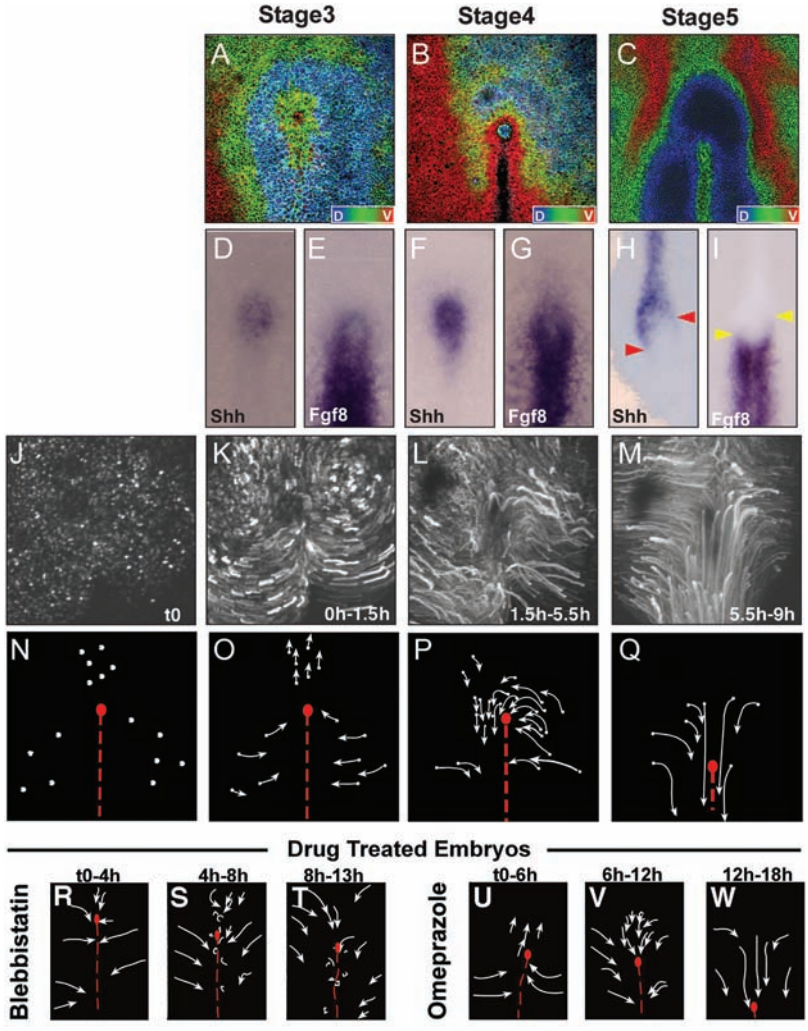

Fig. 1. Morphological and molecular asymmetries arise in conjunction with a leftward movement around the chick at Hensen's node in stage 4. (**A** to **C**) 3D reconstruction of confocal views (Z stack) of phalloidin-stained embryos at stages 3 (A), 4 (B), and 5 (C). The most dorsal (D) staining is depth coded blue; the most ventral (V) staining is shown in red. (**D** to **I**) In situ hybridizations for *Shh* [(D), (F), and (H)] and FGF8 [(E), (G), and (I)]. Red arrows, asymmetric domain of *Shh*; yellow arrows, asymmetric domain of *Fgf8*. (**J** to **M**) Time series showing movement of electroporated cells. (J) Embryos were electroporated at stage 3+, and subsequent time points are indicated in the lower right corner. 10 to 30% of cells are labeled by GFP. Cells undergo a leftward movement around the node (L). White arrows (**N** to **Q**) show the trajectories of the cells depicted in (J) to (M), respectively. In blebbistatin-treated embryos (**R** to **T**), early cell movements are relatively unaffected; however, there is no leftward movement around the node (S). Later, cells display disorganized movements, and the primitive streak fails to regress (T). In omeprazole-treated embryos (**U** to **W**), gastrulation movements are normal; however, cells from the left and right sides move symmetrically toward the node but not around it. The position of the streak and that of the node pit are illustrated by a red dotted line and a red circle, respectively.

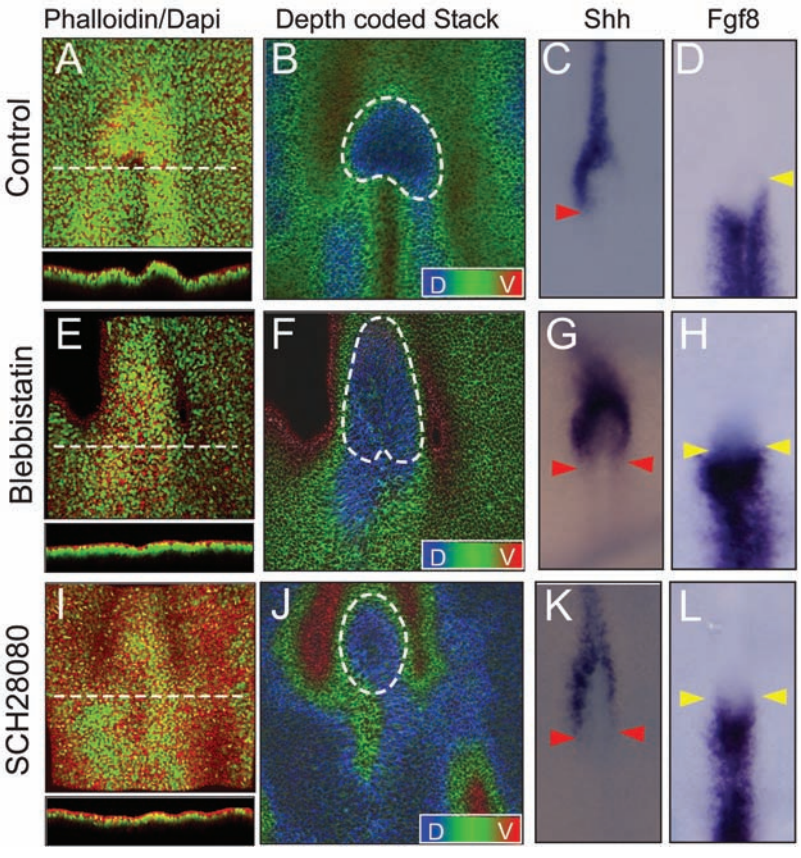

Fig. 2. Effects of myosinII and voltage gradient inhibitors on node morphology and asymmetric expression domains. (**A**, **E**, and **I**) 3D reconstruction of confocal views (Z-stacks) of stage 5 embryos shows the morphology of the node and the primitive streak. Lower panels represent a virtual cross section at the level of the white dotted line. (**B**, **F**, and **J**) Depth-coded 3D reconstruction of confocal views (Z stack) of phalloidin staining. The dorsal-most staining is shown in blue; the ventral-most is shown in red. The shape of the node is outlined by a white dotted shape. In situ hybridization of *Shh* (**C**, **G**, and **K**) and FGF8 (**D**, **H**, and **L**). Red arrows, extent of posterior *Shh* expression; yellow arrows, extent of anterior *Fgf8* expression.

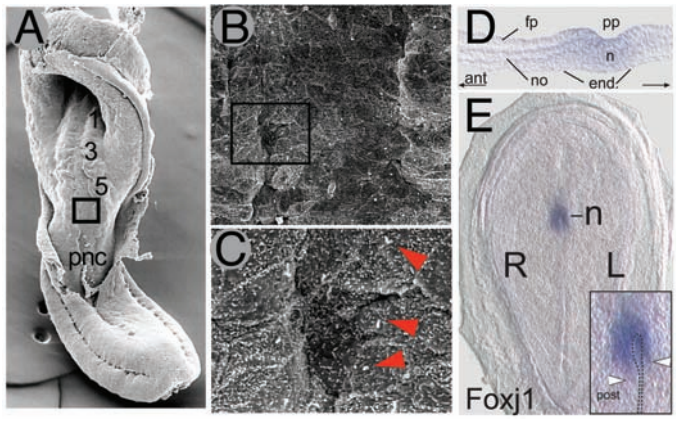

Fig. 3. Similarities between the gastrulation node in the pig embryo and Hensen's node during chick gastrulation. (**A** to **C**) Ventral scanning electron microscopy views of a 5- to 6-somite–stage pig embryo with higher magnifications of the area surrounded by the black box [magnifications shown in (B) and (C)] of the notochordal plate and adjacent paraxial mesoderm. The endoderm forms a continuous ventral cover (that carries short, stubby cilia of 1.5-μm length, indicated by red arrowheads) across the entire ventral surface of the embryo. pnc, prenotochordal cells. (**D**) A sagittal section at the level of the presumptive floor plate (fp) and notochord (no), covered by a continuous layer of endoderm (end). ant, anterior direction (leftward facing arrow); n, node. (**E**) The asymmetric node of a stage 5 pig embryo, marked by asymmetric expression (arrow heads) of the transcription factor Foxj1, demonstrating a shift of the primitive pit (pp, stippled black line). R, right; L, left; post, posterior. For more information, see fig. S4.

As in the chick, we do not observe any structure in the pig resembling the ventral node of the mouse and rabbit. Moreover, as in the chick, the cells of the pig notochordal plate are completely covered by endoderm. As a consequence, there is no space in which a flow of fluid could be generated (Fig. 3E and fig. S4, A and B). Additionally, like the chick, pig embryos have a morphologically asymmetric node displaced leftward at stage 5 (n = 4/4) (Fig. 3C). Like the chick and unlike the mouse, there are asymmetric gene expression domains adjacent to the node, such as Foxj1 (n = 3/3) (Fig. 3A), which precede by several hours the asymmetric expression of Nodal at stage 6 (Fig. 3D). (Nodal is the first gene known to be asymmetrically expressed in mice and rabbits.)

In summary, we show here that, in chick embryos, the node is the site of cellular rearrangements that create a leftward movement of cells around it [an observation made independently by Cui *et al*. (*16*)]. The convergence of cells on the right edge of the node and migration away from the midline on the left thereby deform the shape of the node. This movement establishes asymmetric gene expression patterns, not through transcriptional induction or repression but rather in a passive manner by rearranging the relative orientations of cells expressing critical genes (fig. S5). Moreover, we have found that cell movements at the node arise downstream of a transient depolarization of membrane potential on the left side mediated by the activity of the H+/K+ ATPase. The symmetry-breaking event that leads to asymmetric H+/K+ ATPase activity in chick embroys remains unknown.

Previous misexpression experiments have put the genes asymmetrically expressed at the chick node into an epistatic pathway. For example, according to current models, Bmp4 (which is expressed in very similar domains to *Fgf8*, initially bilaterally along the streak and then asymmetrically on the right side) induces *Fgf8* and represses *Shh*. *Shh* feeds back to repress Bmp4 and induce Nodal, whereas *Fgf8* serves to repress Nodal. Our data do not contradict these previously described epistatic relations. However, because the asymmetric expression domains of these signaling molecules do not form in the absence of cell movements, we suggest that the previously described cross-regulation (for instance, the reciprocal inhibition between *Shh* and Bmp4) functions secondarily to sharpen borders and provide robustness once cells expressing these factors are brought into juxtaposition, rather than as a primary means of establishing their asymmetric gene expression domains.

References and Notes

1. M. Levin, *Mech. Dev.* **122**, 3 (2005).
2. A. Raya, J. C. Belmonte, *Nat. Rev. Genet.* **7**, 283 (2006).
3. J. D. Lee, K. V. Anderson, *Dev. Dyn.* **237**, 3464 (2008).
4. M. L. Kirby *et al*., *Dev. Biol.* **253**, 175 (2003).
5. J. J. Essner *et al*., *Nature* **418**, 37 (2002).
6. Y. Yin *et al*., *Development* **136**, 655 (2009).

7. O. Hertwig, *Lehrbuch der Engwicklungsgeschichte des Menschen und der Wirbelthiere* (Verlag von Gustav Fischer, Jena, Germany, 1910).
8. A. Kölliker, *Entwicklungsgeschichte des Menschen und höheren Thiere* (Wilhelm Engelmann, Leipzig, Germany, 1879).
9. V. Dathe *et al.*, *Anat. Embryol. (Berlin)* **205**, 343 (2002).
10. M. Levin *et al.*, *Cell* **82**, 803 (1995).
11. Materials and methods are available as supporting material on *Science* Online.
12. F. Marlow *et al.*, *Curr. Biol.* **12**, 876 (2002).
13. L. Wei *et al.*, *Development* **128**, 2953 (2001).
14. M. Levin *et al.*, *Cell* **111**, 77 (2002).
15. R. O'Rahilly, F. Muller, *The Embryonic Human Brain: An Atlas of Developmental Stages* (Wiley, Hoboken, NJ, ed. 3, 2006).
16. C. Cui, C. Little, B. Rongish, *Anat. Rec. (Hoboken)* **292**, 557 (2009).

17. We thank M. Levin for helpful suggestions for addressing the role of ion channels; R. O'Rahilly for providing information regarding human embryos; D. Rath and P. Schwartz for provision of pig embryos and assistance with electron microscopy; and C. Cui, C. Little, and B. Rongish for discussing data before publication. This work was supported by a Human Frontier Science Program fellowship to J.G., a Ph.D. fellowship from the Boehringer Ingelheim Fonds to K.F., a grant from the Deutsche Forschungsgemeinschaft (DFG) to M.B., a grant from the DFG (VI 151-8-1) to C.V., and grant R01-HD045499 from NIH to C.J.T.

Supporting Online Material

www.sciencemag.org/cgi/content/full/1172478/DC1
Materials and Methods
Figs. S1 to S6
References
Movies S1 to S6

18 February 2009; accepted 26 March 2009
Published online 9 April 2009;
10.1126/science.1172478
Include this information when citing this paper.

A Frazzled/DCC-Dependent Transcriptional Switch Regulates Midline Axon Guidance

Long Yang, David S. Garbe, Greg J. Bashaw*

Precise wiring of the nervous system depends on coordinating the action of conserved families of proteins that direct axons to their appropriate targets. Slit-roundabout repulsion and netrin–deleted in colorectal cancer (DCC) (frazzled) attraction must be tightly regulated to control midline axon guidance in vertebrates and invertebrates, but the mechanism mediating this regulation is poorly defined. Here, we show that the Fra receptor has two genetically separable functions in regulating midline guidance in *Drosophila*. First, Fra mediates canonical chemoattraction in response to netrin, and, second, it functions independently of netrin to activate *commissureless* transcription, allowing attraction to be coupled to the down-regulation of repulsion in precrossing commissural axons.

Establishing precise midline circuitry is essential to control rhythmic and locomotor behaviors (*1*, *2*). Conserved signals that regulate axon guidance at the midline include attractive cues such as netrins and repulsive cues such as slits, semaphorins, and ephrins (*3*, *4*). In *Drosophila*, netrin attracts many commissural axons to the midline through activation of the frazzled (Fra), the *Drosophila* ortholog of the DCC (deleted in colorectal cancer) receptor (*5*–*8*), whereas the repellant slit and its receptor roundabout (Robo) prevent commissural axons from recrossing (*9*, *10*). Commissureless (Comm) controls midline crossing by negatively regulating surface amounts of Robo on precrossing commissural axons (*11*–*13*). Comm is expressed transiently in commissural neurons as their axons traverse the midline, where it sorts Robo to endosomes (*12*). Once across the midline, *comm* expression is extinguished, resulting in increased amounts of Robo on the growth cone. How *comm* expression is spatially and temporally regulated to gate midline crossing is unknown.

While characterizing the structural requirements for Fra-mediated axon attraction, we observed that neuronal expression of a dominant negative form of Fra (FraΔC) leads to a dose-dependent "commissureless" phenotype (*14*). Searching for candidate genes that modify this phenotype, we found that removing one copy of *comm* enhances the midline-crossing defects caused by expressing *UASFra*Δ*C* (fig. S1), suggesting a role for Fra in regulating Comm during midline guidance. Consistent with this idea, removing one copy of *comm* in hypomorphic *fra* mutants increases the commissural defects as shown by thin or missing commissures in many segments, as well as an increased frequency of noncrossing defects in a subset of commissural neurons: the eagle neurons (Fig. 1 and table S1). Similar genetic interactions are also observed by using additional alleles of both *fra* and *comm* (fig. S2 and table S1). These dose-dependent genetic interactions suggest that *fra* and *comm* may function in the same pathway to control commissural axon guidance.

How could Fra regulate the function of Comm? Because *comm* mRNA is up-regulated in commissural neurons as their axons cross the

Department of Neuroscience, University of Pennsylvania School of Medicine, 1113 BRB2/3, 421 Curie Boulevard, Philadelphia, PA 19104, USA.

*To whom correspondence should be addressed. E-mail: gbashaw@mail.med.upenn.edu

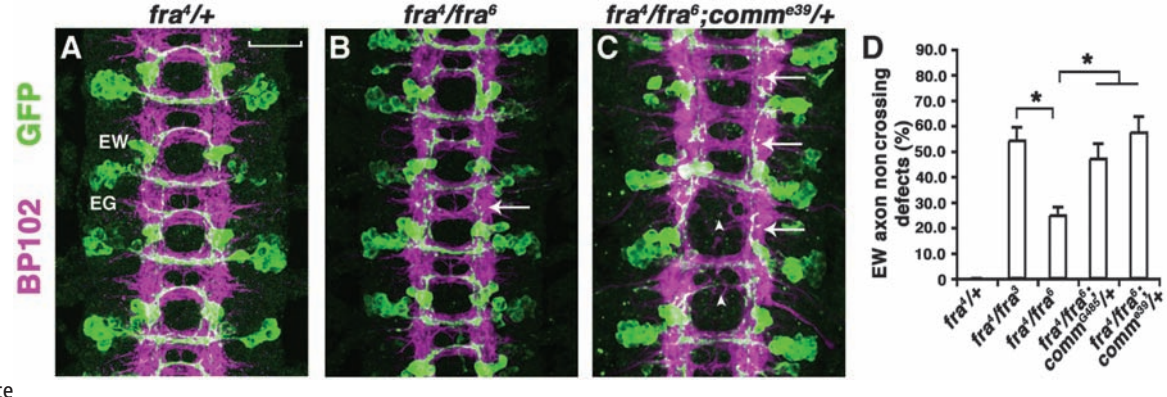

Fig. 1. Genetic interaction between *fra* and *comm*. (**A** to **C**) Stage 16 *eglGal4::UASTau-MycGFP* embryos stained with MAb-BP102 (magenta) to display all central nervous system axons and anti–green fluorescent protein (GFP) (green) to visualize the eagle neurons. Anterior is up. (A) In fra^4/+ or fra^4/+; $comm^{e39}$/+ embryos, EW and EG neurons (white labels) project their axons across the midline in almost every segment. Scale bar indicates 20 μm. (B) fra^4/fra^6 mutants have normal commissure formation and a mild EW axon noncrossing defect (arrow). (C) Compared with fra^4/fra^6, fra^4/fra^6; $comm^{e39}$/+ embryos have missing and thin commissures in many segments (arrowheads), and many EW axons also fail to cross the midline (arrows). (**D**) Quantification of EW axon noncrossing defects. The guidance of EG axons is not affected in *fra* mutants. Error bars represent standard error of the mean. Asterisks denote $P < 0.02$ in a Student's *t* test.

Cell Movements at Hensen's Node Establish Left/Right Asymmetric Gene Expression in the Chick

Jerome Gros, Kerstin Feistel, Christoph Viebahn, Martin Blum, and Clifford J. Tabin

Science, **324** (5929), .
DOI: 10.1126/science.1172478

Migration and Asymmetry

Although vertebrates show asymmetry in internal body organization, the earliest steps toward establishing different anatomies on the left and right sides are not conserved. How this is achieved in birds has been especially confusing. Gros *et al.* (p. 941, published online 9 April) show that in chicks some of the earliest left-right asymmetric domains of gene expression, including those of *Sonic hedgehog (Shh)* and *Fibroblast growth factor 8 (Fgf8)*, are produced passively. Genes are activated in bilateral cell populations, followed by rearrangements that shuffle *Shh*-expressing cells.